Modeling of Basin Type Single Slope Solar Still Under Local Climate Conditions in Yemen

Abdul-Malik Ebrahim Momin[1], Khaled Ali Al-attab[2,*], Mohammed Al-Shaghdari[1], Hamoud Al-Nehari[1]

[1] Mechanical Engineering Department, Faculty of Engineering, Sana'a University, Sana'a, Yemen
[2] School of Mechanical Engineering, Engineering campus, Universiti Sains Malaysia,14300 Nebong Tebal, Penang, Malaysia

ARTICLE INFO	ABSTRACT
	Large-scale membrane water desalination suffers from its high energy penalty with environmental disadvantage of concentrated brine waste. While water evaporation is another alternative for desalination but requires high thermal input that can be obtained using solar collectors. The economic crises and instability caused by the conflict in Yemen prevents the establishment of medium and large-scale water desalination plants to overcome the sever water scarcity in the high population major cities. This paper investigates small scale solar still water desalination technology as a potential candidate to aid with the production of fresh water to reduce the accelerated depletion of underground water reserves in Yemen. Water stills have the advantage of low capital cost and no operational cost as it utilizes the high solar radiation intensity in the coastal areas to evaporate water. This paper proposes and compares two models to simulate the performance of solar still following steady-state and transient modelling approaches, with in-depth evaluation of the different parameters affecting the performance. The transient model showed better prediction of the temperature profiles of the solar still when compared to other experimental and mathematical modelling studies. The small scale solar still showed water production yield of about 1.9 kg/day, with maximum hourly yield of about 0.27 kg/h. The new mathematical model was verified using experimental data and it showed accurate prediction of temperatures inside the still. This model can be used as a general model for water stills with modification on the geometry to provide flexible calculations to optimize the water still geometry for different locations with different solar intensities.

1. Introduction

The utilization of renewable resources not only helps in mitigating environmental issues, but also alleviates some of the economic burdens by providing low-cost energy supply. Recently, new technologies have been proposed for low-cost renewable energy harvesting such as fluid-induced vibration by Ahmadi *et al.,* [1] to utilize wind energy without using conventional rotating wind turbines, solar chamber for drying agriculture product by Hao *et al.,* [2] and biofuels from agriculture

---

* *Corresponding author.*
E-mail address: khaled@usm.my (Khaled Ali Al-attab)

waste by Beriache *et al.,* [3]. Yemen is one of the poorest countries in the world, however, the availability of good wind and solar intensity along the extended cost line from the west to the south makes the use of such renewable energy resources attractive. Yemen has high solar radiation energy intensity of about 27 MJ/m^2/day especially at the costal line with low annual rainfall intensity as reported by Al-Nehari *et al.,* [4]. Yemen is one of the most water-constrained countries in the world where the available water is 80 cubic meters per capita per year as reported by Noaman *et al.,* [5]. This is below the water poverty level of 1,000 m^3/capita/y, with increased concerns regarding the trends of water use while it relies almost exclusively on exploitation of groundwater as reported by Berg *et al.,* [6]. Moreover, according to the World bank data [7], the ongoing conflict significantly affected the GDP, leading to a contraction of nearly 50% in the period of 2011-2023, which resulted in poverty increase and economy and income generation insecurities. This limits the possibilities for any government or private projects for water desalination due to the high initial and operational costs needed when using conventional seawater desalination methods. The use of novel materials for water treatment can effectively remove impurities and control water pH as reported by Huang *et al.,* [8], however, normal water treatment without special membranes is not adequate for water desalination. Water desalination theory can be divided into two main categories: thermal-based and membrane-based. Most common technologies under thermal-based desalination include multi-stage flash, multi-effect desalination (MED), vapor compression and solar still desalination, while for membrane-based include reversed osmosis, membrane nanofiltration and electrodialysis as reviewed in a recent study [9]. The neighboring countries within the Gulf Cooperation Council (GCC) hold up to 43% of the share capacity of total global desalination with nearly 16 thousand desalination plants which utilize all of the above-mentioned desalination technologies. Therefore, impact of the technologies used can be highlighted by means of their environmental impact from brine production and total CO_2 emissions additional to the energy cost of the process as reported by Moossa *et al.,* [10]. Hiving brine as a by-product from desalination is a big concern as it contains a high concentration of dissolved solids along with other pollutants, so it cannot be directly discharged to the environment. Therefore, brine management through additional hypersaline desalination becomes a necessity to avoid its adverse effects on environment as reported by Shah *et al.,* [11]. Moreover, concerns have been raised by researchers [12] on the rapid increase of the Gulf seawater desalination plants and their negative effects on coastal ecosystem if these plants continue the business-as-usual strategy without adopting sustainable solutions. Thermal based MED was proposed due to its considerably lower energy consumption by many researchers to be used with renewable power sources such as wind or PV solar panels, however, additional cost has to be considered for the needed electrical energy storage. To overcome the necessity of energy storage, geothermal can be used as a direct heat source since MED is well suited for low temperature heat input sources as shown in a recent study [13]. As a long-term plan when the economy recovers in Yemen after the conflict is resolved, solar-powered large-scale desalination plants can be implemented. However, for the short and medium terms, desalination plant cost is a major factor which limits the possibility of using electrical storage batteries for large scale freshwater production. Nevertheless, solar energy can still be used as a thermal source for desalination. Elaborate research has been done by researchers [14] on solar collectors for thermal applications with emphasis on the properties of the primary heat transfer fluid where nano-fluids have shown considerable enhancement on the collector performance.

Solar stills have been widely studied as low-cost small-scale distributed water desalination units. The simplest base design is the inclined still with single glazing surface as simulated by a recent study [15]. Main factors that affect the solar still are the basin geometry and the glazing surface inclination angle as reported by Essa *et al.,* [16]. Adding external solar collectors to enhance the evaporation

was investigated where two geometries of finned tube and flat plate solar collector were compared by Abdulridha *et al.,* [17]. However, adding external collectors increases the cost of the system while the enhancement on the production yields was not significant where conventional solar still alone, and with flat plate and finned tubes provided 2.8, 3.8 and 4.7 L/m^2.day, respectively. Another way suggested by Sahota *et al.,* [18] to enhance the still production is by increasing the glazing area on the still done by using two surfaces in double slope design, or four surfaces in pyramid design by Sharshir et al., [19] with additional reflectors to increase the solar radiation intensity. It was reported in a recent study [20] that Solar stills are cheap, simple and need low maintenance, but they suffer from low freshwater productivity. A study [19] tested the addition of wick or other solid porous materials and also fins were added in another study [21] to the solar absorber to increase the contact heat transfer surface area with water and also having energy storage capability to elevate the temperature. The temperature of the glazing glass must be lower than the water condensation, otherwise, moist air is transferred to external condenser using a fan which adds some operational cost to the system as reported by Rabhi *et al.,* [21]. In order to increase the production rate of fresh water per floor unit area, vertical glazing glass was proposed by Abbaspour *et al.,* [22] since the height can be extended with the addition of multi-effect layers to recover heat and increase efficiency. Also, a wide range of techniques to reduce heat losses from solar still walls were reviewed by Omara *et al.,* [23]. Experimental testing of multi geometries is not only costly but also time consuming as a single data collection can only be achieved through an entire day of operation. Numerical analysis, on the other hand, can be performed at a significantly lower cost and shorter time. Numerous numerical programs are in use by engineers and scientists around the world. These programs can be categorized as either special-purpose or general-purpose numerical programing. A special purpose program was developed Madhlopa and Johnstone [24] to simulate a specific process, with low flexibility, where changes to the process may demand extensive modifications to the program. Nevertheless, the advantage of a special purpose program is the simplicity of developing a mathematical model that adequately describes a real system. Codes are commonly written using programming languages such as BASIC, FORTRAN, Pascal and MATLAB.

In this study, a new mathematical transient model was developed to simulate full operation sun cycle of single basin solar still through dynamic heat and mass transfer inside and outside the still. Full parametric characterization was performed to investigate the effect of the climatic, design and operational parameters on the performance and the change in daily distillate production of the system. The model is compared with the classical steady-state heat balance and was verified using experimental data. This model is a step towards flexible optimization of water still geometry and operating conditions for different locations with different solar intensities that can be utilized by other researchers following this model methodology and calculations.

2. Numerical modeling

Two models are compared in this study, first steady state model and transient model as will be discussed in the following sections.

2.1 Steady State Model

In this model an energy balance is applied for different parts of the still. It is always assumed that all parts are at quasi-steady state. Theoretically it is found that the daily distillate production is more than doubled for a typical set of parameters as the glass cover temperature is promptly reduced, which accelerates water condensation rate. The effect of the climatic (y), design (L) and operational

(u) parameters on the performance of the system have been evaluated. Numerical calculations were made for a typical day in Sana'a, Yemen. First, an energy balance of the whole still is applied, Figure 1 in which all interactions with the outside is considered. Such a balance is shown below:

Fig. 1. Energy balance of the solar still

The general assumptions for the steady state modeling that are commonly acceptable for solar collectors were reported by Duffie and Beckman [25] and considered for this study as following:

i)   There is no vapour leakage in solar still.
ii)   It is an air tight basin, hence no heat loss.
iii)   Heat capacity of cover and absorbing material, insulation can be negligible.
iv)   There is no temperature gradient across the basin and glass cover of solar still.
v)   Water level inside the basin can be maintained at constant level.
vi)   The control volume encloses the whole still and the outside air has a constant uniform speed.

The solar radiation intensity (I^*_s) is calculated using Eqs. (1) & (2) obtained from the reference study [25]:

$$I^*_s A_g = I^*_s * r_g * A_g + q^*_{g,s} * A_g + q^*_{h,g} * A_g + q^*_{k,air} * A_{k,air} + q^*_{k,l} A_{k,l} + q^*_{k,b} A_b + \left(m^*_{cw} h_{sat,g}\right) \tag{1}$$

$$\frac{I^*_s A_g}{A_b} = I^*_s * r_g * \frac{A_g}{A_b} + q^*_{g,s} * \frac{A_g}{A_b} + q^*_{h,g} * \frac{A_g}{A_b} + q^*_{k,air} * \frac{A_{k,air}}{A_b} + \frac{q^*_{k,l} A_{k,l}}{A_b} + \frac{q^*_{k,b} A_b}{A_b} + \frac{m^*_{cw} h_{sat,g}}{A_b} \tag{2}$$

where I^*_s the solar radiation intensity and r_g is the reflectivity of the glass cover. The heat stored in the glass cover is then transferred from the cover to the atmosphere through convection using the general sensible heat balance Eq. (3):

$$q^*_{h,g} = h_g\left(T_g - T_a\right) \tag{3}$$

where T_g is the glass temperature, h_g is the convective heat transfer coefficient which is calculated using Eq. (4) provided by Duffie and Beckman [25]:

$$h_g = 2.8 + 3V_w \tag{4}$$

where the forced convection coefficient is dependent on the wind velocity V_w (m/s). Some of the heat is also transferred to the atmospheric air through radiation which is calculated using Eq. (5) provided by Duffie and Beckman [25]:

$$q^*_{g,s} = \varepsilon_g C_s \left[(T_g/100)^4 - (T_{sky}/100)^4 \right] \tag{5}$$

where the emissivity of the glass, ε_g, is 0.88 for infrared radiation, the constant, C_s, is $5.667 \, \text{W/m}^2\text{K}^4$ and T_{sky} is the sky temperature. Generally, for practical purposes it can be assumed to be related to the ambient temperature and which can be calculated using Eq. (6) provided by Duffie and Beckman [25]:

$$T_{sky} = 0.0552 * T_a^{1.5} \tag{6}$$

The conductive heat transfer from the bottom to the atmosphere may be calculated using standard conduction heat transfer Eq. (7):

$$q^*_{k,b} = k_b(T_b - T_a) \tag{7}$$

where standard Eq. (8) of thermal resistance calculation is used to calculate the overall thermal conductivity (kb):

$$\frac{1}{k_b} = \frac{1}{h_m} + \sum \frac{\delta_i}{\lambda_i} + \frac{1}{h_a} \tag{8}$$

Similarly, the calculation of the conduction heat transfer from the circumferential area of the still from the inner moist air to the atmosphere, followed by the calculation of heat transfer from liquid to the atmosphere, all use standard Eqs. (9-12) for conduction and thermal resistance:

$$q^*_{k,air} = k_r(T_r - T_a) \tag{9}$$

$$\frac{1}{k_r} = \frac{1}{h_r} + \sum \frac{\delta_i}{\lambda_i} + \frac{1}{h_a} \tag{10}$$

$$q^*_{k,l} = k_l(T_l - T_a) \tag{11}$$

$$\frac{1}{k_l} = \frac{1}{h_l} + \sum \frac{\delta_i}{\lambda_i} + \frac{1}{h_a} \text{ and } T_l = \frac{T_i + T_b}{2} \tag{12}$$

where $h_{sat,g}$ is the enthalpy of water at saturation temperature T_g and m^*_{cw} is the mass flow rate of condensed water. After that, the energy balance for the glass cover shown in Figure 2 is calculated starting with the solar radiation intensity from Eqs. (13) & (14) provided by Duffie and Beckman [25]:

$$I^*_s A_g + q^*_{i,g} * A_g \cos\beta + q^*_{h,r} * A_g + m^*_{m,air} h_{m,air,r} = I^*_s r_g A_g + I^*_s d_g A_g + q^*_{g,s} A_g +$$
$$q^*_{h,s} A_g + q^*_{\lambda,gh} A_{\lambda,gh} + q^*_{h,gf} A_{h,gf} + m^*_{cw} h_{sat,g} \tag{13}$$

$$I^*_s A_g/A_b + q^*_{i,g} * A_g/A_b \cos\beta + q^*_{h,r} * A_g/A_b + m^*_{m,air} h_{m,air,r}/A_b = I^*_s r_g A_g/A_b + I^*_s d_g A_g/$$
$$A_b + q^*_{g,s}A_g/A_b + q^*_{h,s}A_g/A_b + q^*_{\lambda,gh}A_{\lambda,gh}/A_b + q^*_{h,gf}A_{h,gf}/A_b + m^*_{cw} h_{sat,g}/A_b \qquad (14)$$

where $q^*_{i,g}$ is the radiative heat flux from the water surface to the glass, $q^*_{h,r}$ is the convective heat flux from the water surface to the glass and $h_{m,air}$ is the enthalpy of water at saturation temperature T_r and $m^*_{m,air}$ is the mass flow rate of moist air. $q^*_{\lambda,gh}$ and $q^*_{h,gf}$ are the heat losses from the back and front borders of the glass and for calculations they can be neglected.
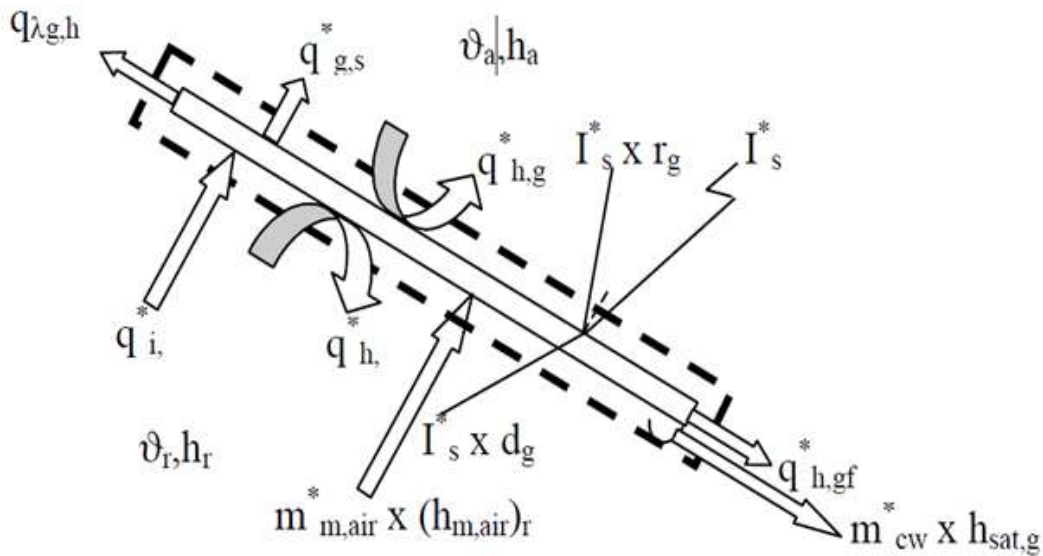
Fig. 2. Energy balance of the glass cover

Between an optical permeable and non-permeable walls where water surface is assumed to be a non-permeable wall because transmittance of water equals zero for infrared radiation, radiative heat transfer from the water to the glass is calculated using Eq. (15) provided by Cengle and Ghajar [26]:

$$q^*_{i,g} = \frac{\left[\left(\frac{T_i}{100}\right)^4 - \left(\frac{T_g}{100}\right)^4\right]}{\frac{1}{\varepsilon_g C_s} + \frac{1}{\varepsilon_w C_s} - \frac{1}{C_s}} \qquad (15)$$

where ε_w is the emissivity of water. Convective heat transfer from the water to the glass is then calculated using standard convection heat transfer Eq. (16):

$$q^*_{h,r} = h_r(T_r - T_g) \qquad (16)$$

where h_r, is the convective heat transfer coefficient which is calculated based on Nusselt number calculations in Eqs. (17-19) and Grashof number, Gr, calculation Eq. (20) provided by Cengle and Ghajar [26]:

$$Nu = 0.766[Raf_2(\text{Pr})]^{1/5} \, for: \, Raf_2(\text{Pr}) \leq 7 \times 10^4 \qquad (17)$$

$$Nu = 0.15[Raf_2(\text{Pr})]^{1/3} \, for: \, Raf_2(\text{Pr}) \geq 7 \times 10^4 \qquad (18)$$

$$f_2(\text{Pr}) = \left[1 + (0.322/Pr)^{11/20}\right]^{-20/11} \qquad (19)$$

$$Gr = \frac{gl^3}{v^2}\beta\Delta T \tag{20}$$

where g (m/s^2) is the gravitational acceleration, v (m^2/s) is the momentum diffusivity, l (m) is the characteristic length, which is calculated using geometry calculation in Eq. (21):

$$l = \frac{A}{U} \tag{21}$$

where A (m^2) is the surface area and U (m) is the circumference of the participating heat transfer area projected in downstream direction.

An important thermodynamic property of the fluid, which is the thermal expansion coefficient, β, calculated using Eq. (22), provides a measure of the amount by which density changes in response to a change in temperature at constant pressure, which can be expressed in approximate form using Eq. (23) provided by Cengle and Ghajar [26]:

$$\beta = -\frac{1}{\rho}\left(\frac{\partial\rho}{\partial T}\right)_P \tag{22}$$

$$\beta\Delta T = -\frac{1}{\rho}\frac{\rho_\infty - \rho_0}{\rho_\infty} \; valid \; for \; \beta\Delta T \ll 1 \tag{23}$$

where ρ_0 is the inside density while ρ_∞ is the outside density of the boundary layer. Free convection effects obviously depend on the expansion coefficient β calculated in Eq. (24) at the respective reference temperature, while Rayleigh number is calculated using Eq. (25), provided by Cengle and Ghajar [26]:

$$\beta = \frac{1}{273}[K^{-1}] \quad or \quad \beta = \frac{1}{T_\infty}[K^{-1}] \tag{24}$$

$$Ra = Gr * Pr \tag{25}$$

For all calculations, the physical and transport properties will be at mean temperature T_m Eq. (26):

$$T_m = \frac{T_0 + T_\infty}{2} \tag{26}$$

Knowing the thermal conductivity, λ, of air at T_m, the convective heat transfer coefficient can be calculated using standard equation Eq. (27):

$$h_r = \frac{Nu\lambda}{l} \tag{27}$$

Energy balance of the water interface is shown in Figure 3 with the control volume enclosing the top layer of the water.
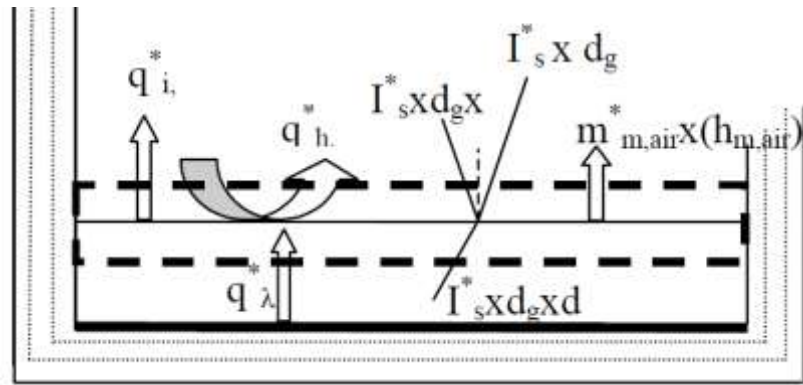
Fig. 3. Energy balance of the water interface

The energy balance calculations for seawater interface starts from the solar radiation intensity calculations are shown in Eqs. (28) & (29) provided by Duffie and Beckman [25]:

$$I^*_s \, d_g \, A_b + \, q^*_\lambda \, A_b = I^*_s \, d_g \, r_w \, A_b + I^*_s \, d_g \, d_w \, A_b + q^*_{i,g} \, A_b + q^*_{h,r} \, A_b + \left(m_{m,air} \, h_{m,air,i} \right) \quad (28)$$

$$I^*_s \, d_g + \, q^*_\lambda = I^*_s \, d_g \, r_w + I^*_s \, d_g \, d_w + q^*_{i,g} + q^*_{h,r} + \frac{m_{m,air} \, h_{m,air,i}}{A_b} \quad (29)$$

where d_w is the transmittance of water, r_w is the reflectivity of water for visible light, $h_{m,air}$ is the enthalpy of water at saturation temperature. The heat transfer from the bottom to the seawater interface is calculated using the standard conduction Eq. (30), while the heat transfer from seawater interface to the glass cover is calculated using the standard convection Eq. (31):

$$q_\lambda = \frac{\lambda_w}{\delta_w} (T_b - T_i) \quad (30)$$

$$q_{h,r} = h_r (T_i - T_r) \quad (31)$$

Finally, the energy balance for the basin with the close system enclosing the metallic basin alone is shown in Figure 4.
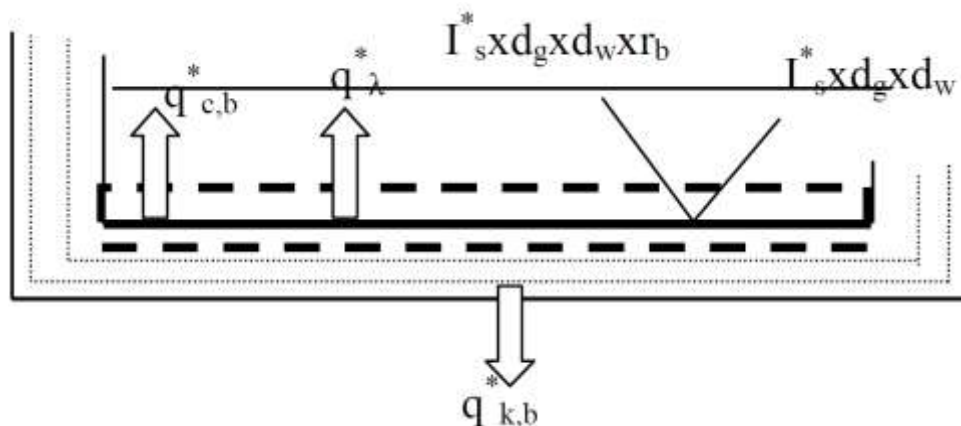
Fig. 4. Energy balance of the basin liner

The energy balance calculations for black plate are shown in Eqs. (32) & (33) provided by Duffie and Beckman [25]:

$$I^*_s \, d_g \, d_w \, A_b - I^*_s \, d_g \, d_w r_b \, A_b = q^*_\lambda \, A_b + q^*_{k,b} \, A_b + q^*_{c,b} \, A_b \tag{32}$$

$$I^*_s \, d_g \, d_w - I^*_s \, d_g \, d_w r_b = q^*_\lambda + q^*_{k,b} + q^*_{c,b} \tag{33}$$

where r_b is the reflectivity of black plate, $q^*_{c,b}$ is the heat transfer from bottom wall to the seawater layer calculated using the standard convection Eq. (34):

$$q^*_{c,b} = h_{cb}(T_b - T_i) \tag{34}$$

As the depth of seawater layer is very limited, convective heat transfer from the black plate through the seawater can be neglected. Reynolds analogy holding mass transfer coefficient is calculated using Eq. (35) provided by Duffie and Beckman [25]:

$$h_M = \frac{h}{\rho c_p} \left[\frac{m}{s}\right] \tag{35}$$

The mass flow rate of evaporated water is then calculated according to the semi-permeable plane theory. For this purpose, first, the mass flux for a non-permeable plane according to the Reynolds analogy is calculated. Using this value, the mass transfer coefficient for semi permeable plane is calculated using Eq. (36) provided by Duffie and Beckman [25]:

$$h_{M,h} = h_M \frac{P}{P_i - P_r} \ln \frac{P - P_r}{P - P_i} \tag{36}$$

And then mass flow rate of evaporated water mass is calculated using Eq. (37) provided by Duffie and Beckman [25]:

$$m_{vapor} = h_{M,h} \frac{1}{RT} (P_{v,w} - P_{v,air}) A_b \left[\frac{kg}{s}\right] \tag{37}$$

2.2 Energy Balance Program for Steady State Model

Following the suggestions of previous study by Madhlopa [31], the following assumptions were made for the theoretical modeling of the solar still:

i) The whole system is in a quasi-steady state condition.
ii) Heat loss by radiation from the circumferential area is neglected.

A code was written in C language to simulate this model iterations. Flow chart and algorithm of the solution procedure of the first model are illustrated in Figure 5. The modeling procedure is initiated by collecting the weather conditions, thermal properties and design parameters of the still. This is assumed by assuming initial values of the four main temperatures of the glass cover (Tg), inner air (Tr), interface (Ti) Bottom (Tb). At the base of the still, temperature of the walls is in equilibrium with water temperature, where the average of the interface water temperature and the bottom temperature is considered. The wind speed is assumed to be constant during the experiment. Temperature related thermal properties are then calculated at these temperatures, these and all other variables are then substituted in Eqs. (38-41) for f1, f2, f3, f4. The homogeneous temperature functions are set to zero.

f1(Tr,Tb,Ti,Tg)=0 (38)

f2(Tr,Tb,Ti,Tg)=0 (39)

f3(Tr,Tb,Ti,Tg)=0 (40)

f4(Tr,Tb,Ti,Tg)=0 (41)

The summation of the squares of these energy function equations are calculated and compared to an allowance factor of the order (e^{-25}). This condition cannot be satisfied in the initial run of the first iteration of the calculation loop in the program, and the iterations are continued until the conditions are met. The gradient of the energy function taken for each variable are then calculated. Each variable is then assigned to approximate values by subtracting a convenient number from the original initial value, this convenient number is the multiplication of the gradient of the energy function by a small number called the learning rate (taken as e^{-08}). Then the whole process is repeated through the calculation loop until the criterion of the allowance factor is met. Finally, all values of temperatures and evaporated mass flow rate are reported.
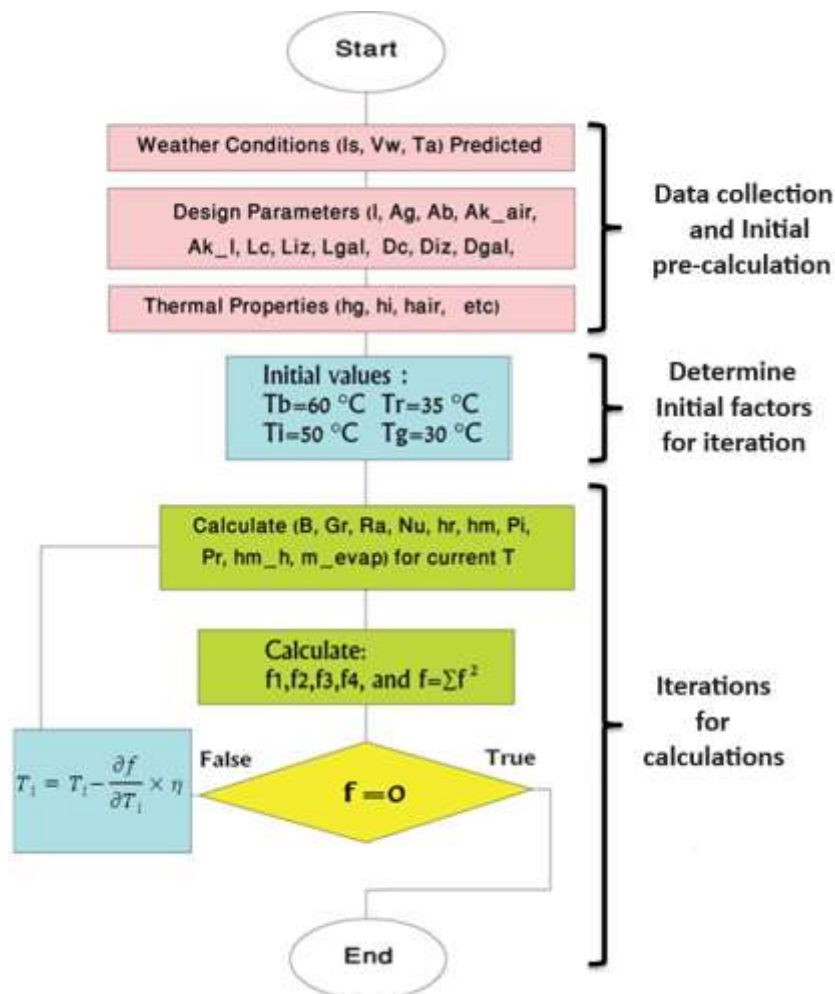
Fig. 5. Flow chart and algorithm of the solution procedure of the first model

2.3 Transient Model

In this model, time effects are taken into account and the transient heat conduction equation through walls is applied for the glass, water layer, and basin. The lumped system analysis concept will be applied for these parts, and its applicability will be discussed in the following sections. It must be noted that in this model, the inner moist air temperature cannot be considered as an independent variable in lump system concept. Thus, air temperature will be assumed to be an average value between the water and the glass temperature, but the water temperature is given a higher weight though. As water gets heated it transfers part of its energy into the cold air above through two mechanisms, convection and diffusion or humidification. The air then undergoes an increase in temperature alongside an increase in its humidity through sensible and latent heating, yielding a high energy transfer rate. On the other side however, near the glass, the process takes place on a very slow pace. Thus, the air temperature builds up with time closer to the water temperature. The nodal points and relevant temperatures, thermal resistances through each connected node, and the energies fed into each node are illustrated in Figure 6, while the different symbols are explained in Table 1.
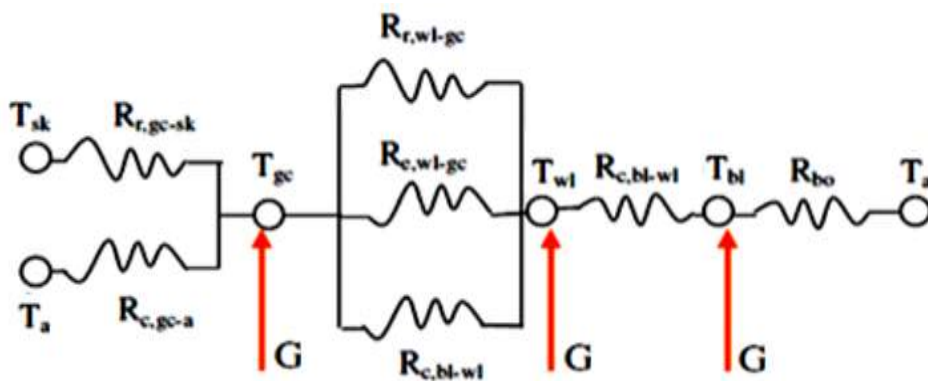
Fig. 6. Nodal diagram showing thermal resistance used in the solar still model

Table 1
Thermal resistance (TR) for each part of the system

Symbol	Definition
Rc, gc-a	Convective TR between glass cover and ambient air
Rr, gc-sk	Radiative TR between glass cover and sky
Rc, wl-gc	Convective TR between water and glass
Rr, wl-gc	Radiative TR between water and glass
Re, wl-gc	Evaporative TR between water and glass
Rc, bl-wl	Convective TR between basin and water
Rbo	Conductive TR of the basin, insulation, and outer frame materials

The transient one-dimensional heat conduction equation, when applied to a body with neglected spatial temperature gradients, utilizes the lumped capacitance method to calculate the variation of temperature with time. So, the general heat balance Eq. (42) for a solid structure with convective and radiative heat loss from its surface is then calculated.

$$\rho V' C \frac{dT}{dt} = Q_{es} + Q_{ig} - [h_c(T - T_a) + \varepsilon\sigma(T^4 - T_{sr}^{\;4})] \tag{42}$$

If the structure does not generate heat internally (Qig = 0) with no heat flow from an external source (Qes = 0), then the general heat balance correlation is reduced to Eq. (43):

$$\rho V'C \frac{dT}{dt} = -[h_c(T - T_a) + \varepsilon\sigma(T^4 - T_{sr}^4)] \tag{43}$$

The application of the lumped capacitance method depends on the Biot number (Bi), given by Eq. (44) provided by Cengel and Ghajar [26], where $Bi \leq 0.1$:

$$Bi = \frac{T_1 - T_2}{T_2 - T_a} = \frac{h_c L}{k} \tag{44}$$

A finite difference equation is written for each node in the nodal network, reducing the system to a set of linear algebraic equations, which can then be solved directly or iteratively. Direct methods include backward substitution, Gaussian elimination and matrix inversion, which are suitable for a small number of equations. It should also be mentioned that a finite difference equation can be expressed in an explicit or implicit form. One drawback of the explicit method is its conditional stability as reported by Incropera *et al.,* [27]. As the time step increases, the solution may oscillate significantly from the steady-state conditions resulting in huge errors. In contrast, the convergence of a solution is unconditional in an implicit approach. For instance, one-dimensional heat transfer equation can explicitly be discretized as shown in Eq. (45). The equations for this model calculations are provided by Incropera *et al.,* [27].

$$\frac{1}{\alpha'} \frac{T_i^j - T_i^{j-1}}{\Delta t} = \frac{T_{i+1}^{j-1} + T_{i-1}^{j-1} - 2T_i^{j-1}}{(\Delta x)^2} \tag{45}$$

where i = 1,2,3 … and j = 1,2,3, …, and solving for the interior i^{th} nodal temperature at the jth time step yields the following Eq. (46):

$$T_i^j = F'\left(T_{i+1}^{j-1} + T_{i-1}^{j-1}\right) + (1 - 2F')T_i^{j-1} \tag{46}$$

where F' is the mesh Fourier number, which is calculated using Eq. (47):

$$F' = \frac{\alpha' \Delta t}{(\Delta x)^2} \tag{47}$$

Note that when $F' = 0.5$, the explicit finite difference formulation for a general interior node reduces to $T_i^j = \left(T_{i+1}^{j-1} + T_{i-1}^{j-1}\right)/2$ which has the interesting interpretation that the temperature of an interior node at the new time step is simply the average of the temperatures of its neighboring nodes at the previous time step. The accuracy of the finite difference method can be improved by decreasing the sizes of Δx and Δt. This increases the number of interior nodes and time steps and the computational time. So, the choice of mesh size is based on the accuracy and computational demands. In addition, stability constraints may be used to select the right values of Δx and Δt. For one dimensional interior node, the stability requirement is ($F' \leq \frac{1}{2}$) as reported by Cengel and Ghajar [26]. Consequently, Δt can be determined for fixed values of Δx and α'. It should also be mentioned that the one-dimensional heat equation can implicitly be discretized to the following correlation Eq. (48):

$$\frac{1}{\alpha'} \frac{T_i^j - T_i^{j-1}}{\Delta t} = \frac{T_{i+1}^j + T_{i-1}^j - 2T_i^j}{(\Delta x)^2} \tag{48}$$

Solving the implicit finite difference equation for the interior i^{th} nodal temperature at the jth time step gives Eq. (49):

$$T_i^j = \frac{T_i^{j-1} + F'\left(T_{i+1}^j + T_{i-1}^j\right)}{(1 + 2F')} \tag{49}$$

One of the advantages is that there is no stability criterion for the implicit scheme because the solution is unconditionally stable. Lager values of Δx and Δt can be used with this method, thereby reducing the computational time. The final task in the simulation process is to solve the system of discretized equations which requires an appropriate computational platform.

2.4 Energy Balance Program for Transient Model

The proposed model for calculating the distribution of solar energy inside a solar still was applied to the single basin single slope solar still. The assumptions that are commonly acceptable for transient modeling solar collectors as reported by Duffie and Beckman [25] were considered for this study as following:

i)   The solar still is assumed to be airtight.
ii)   Solar radiation intercepted by the exterior surfaces of the walls is neglected.
iii)   No leakage of vapor and distilled water from the systems.
iv)   Mass change (with time) of saline water in the basins is negligible.
v)   Saturation degree of the air and its ability of absorbing more water are also neglected. In other words, the evaporated water can be condensed elsewhere or, as a mass (m) of water is evaporated (within the water-air interface), the same mass is condensed at the glass inner surface.

With these assumptions, the energy balance equations for each component of the solar still are then calculated. First, energy balance for the glass cover is calculated using Eq. (50) provided by Duffie and Beckman [25]:

$$m_{gc}C_{p,gc}\frac{dT_{gc}}{dt} = A_{gc}F_{gc}G_g + A_w h_{gc}(T_w - T_{gc}) - A_{gc}h_{c,gc-a}(T_{gc} - T_a) - A_{gc}h_{r,gc_{sk}}(T_{gc} - T_{sk}) \tag{50}$$

where: $h_{gc} = \left(h_{c,w-gc} + h_{e,w-gc} + h_{r,w-gc}\right)$. Second component is the basin liner Eq. (51):

$$m_b C_{p,b}\frac{dT_b}{dt} = A_w[F_b G_g - h_{c,b-w}(T_b - T_w) - U_{bo}(T_b - T_a)] \tag{51}$$

Third component is water Eq. (52):

$$m_w C_{p,w}\frac{dT_w}{dt} = A_w\left[F_w G_g + h_{c,b-w}(T_b - T_w)\right] - A_w h_w(T_w - T_{gc}) - A_s U_{sw}(T_w - T_a) \tag{52}$$

where: $h_w = h_{gc}$. However, when augmenting the still with evacuated tubes, this equation must be modified to include the effect of the tubes which provide excess energy to the water in the basin. The amount of this excess energy delivered by the tubes to the water is: $(\text{Tube Area} \times$

Tube Efficiency $\times G_g$), while the mass of the water in the equation is modified to ($m_{(w+)} = m_w + N_p D_p^2 (\frac{\pi}{4}) L_p \times \rho_w$). Therefore, the modified equation will become Eq. (53):

$$m_{(w+)} C_{p,w} \frac{dT_w}{dt} = A_w [F_w G_g + h_{c,b-w}(T_b - T_w)] + N_p D_p L_p \eta_{tube} G_g - A_w h_w (T_w - T_{gc}) - A_s U_{sw}(T_w - T_a) \tag{53}$$

where N_p is number of evacuated tubes, D_p is inner diameter of the evacuated tubes, L_p is length of the evacuated tube and η_{tube} is the efficiency of the evacuated tube ranging from 30 to 45%. Solar radiation is attenuated as it propagates through the glass cover and saline water to reach the basin liner. These still components absorb part of the radiation, and the values of the solar absorption factors should be computed by considering the angular dependence of solar transmission and absorption through a glass cover shown in Eqs. (54-56) provided by Zurigat and Abu-Arabi [28]:

$$F_{gc} = \alpha_{gc} \tag{54}$$

$$F_{w1} = \alpha_{w1} \tau_{gc} \tag{55}$$

$$F_{b1} = \alpha_{b1} \tau_{gc} \tau_{w1} \tag{56}$$

As for the thermal losses from the bottom wall of the still, the heat transfer coefficient is calculated using Eq. (57) provided by Incropera *et al.,* [27]:

$$U_{bo} = \frac{1}{R_{bo}} = \frac{1}{R_{ps}+R_{pw}} = \{\frac{X_{ps}}{k_{ps}} + \frac{X_{pw}}{k_{pw}}\}^{-1} \tag{57}$$

System calculations are based on transient and non-linear differential equations. In view of this, a finite difference method was used to discretize the equations implicitly to obtain a system of linear algebraic equations for the (j^{th}) time step by Incropera et al., [27]. The algorithm of the solution procedure program flowchart is illustrated in Figure 7. The numerical solution procedure starts with the collection of the design parameters of the still, followed by the estimation of the three basic temperature variables (T_w, T_g, T_b) at the early morning for the glass cover, basin liner and water in basin, respectively. The equations used for temperature calculation of these three components are shown in Table 2. The equations were simplified from the reference studies [23, 25-28]. Initially, thermal properties related to the initial temperature values are calculated, which eliminates the effect of the time step on the accuracy of the solution at this stage. This is followed by the calculation of the actual temperature values for each time step (Δt) throughout the day though an iterative calculation loop process for each time step. The iteration loop is stopped once the iterative process reaches a state where temperature does not change within an order of (e^{-08}), and the output value is taken one time step ahead through the second calculation iterative loop of time steps. This iteration loop is continued until the time limit is reached which is the ratio between the sunshine duration and the length of the time-step (time limit = (day–length in seconds)/Δt).

Table 2
Time-step based equations for temperature calculation for the different components of the solar still [23,25-28]

Component	Equation
Glass cover (gc)	$T_{gc}^j = a_{10} + a_{11}T_{gc}^{j-1} + a_{12}T_w^j$
	$a_{10} = \dfrac{\Delta t(A_{gc}F_{gc}G_g + A_{gc}h_{c,gc-a}T_a + A_{gc}h_{r,gc-sk}T_{sk})}{\Delta t(A_w h_{gc} + A_{gc}h_{c,gc-a} + A_{gc}h_{r,gc-sk}) + m_{gc}C_{p,gc}}$
	$a_{11} = \dfrac{m_{gc}C_{p,gc}}{\Delta t(A_w h_{gc} + A_{gc}h_{c,gc-a} + A_{gc}h_{r,gc-sk}) + m_{gc}C_{p,gc}}$
	$a_{12} = \dfrac{\Delta t A_w h_{gc}}{\Delta t(A_w h_{gc} + A_{gc}h_{c,gc-a} + A_{gc}h_{r,gc-sk}) + m_{gc}C_{p,gc}}$
Basin liner (b)	$T_b^j = a_{20} + a_{21}T_b^{j-1} + a_{22}T_w^j$
	$a_{20} = \dfrac{\Delta t A_w(F_b G_g + U_{bo}T_a)}{\Delta t A_w(h_{c,b-w} + U_{bo}) + m_b C_{p,b}}$
	$a_{21} = \dfrac{m_b C_{p,b}}{\Delta t A_w(h_{c,b-w} + U_{bo}) + m_b C_{p,b}}$
	$a_{22} = \dfrac{\Delta t A_w h_{c,b-w}}{\Delta t A_w(h_{c,b-w} + U_{bo}) + m_b C_{p,b}}$
Water in basin (w)	$T_w^j = a_{30} + a_{31}T_w^{j-1} + a_{32}T_{gc}^j + a_{33}T_b^j$
	$a_{30} = \dfrac{\Delta t(A_w F_w G_g + A_s U_{sw}T_a + N_p D_p L_p \eta_{tube}G_g)}{\Delta t A_w(h_{c,b-w} + h_w) + \Delta t A_s U_{sw} + m_w C_{p,w}}$
	$a_{31} = \dfrac{m_w C_{p,w}}{\Delta t A_w(h_{c,b-w} + h_w) + \Delta t A_s U_{sw} + m_w C_{p,w}}$
	$a_{32} = \dfrac{\Delta t A_w F_w}{\Delta t A_w(h_{c,b-w} + h_w) + \Delta t A_s U_{sw} + m_w C_{p,w}}$
	$a_{33} = \dfrac{\Delta t A_w h_{c,b-w}}{\Delta t A_w(h_{c,b-w} + h_w) + \Delta t A_s U_{sw} + m_w C_{p,w}}$
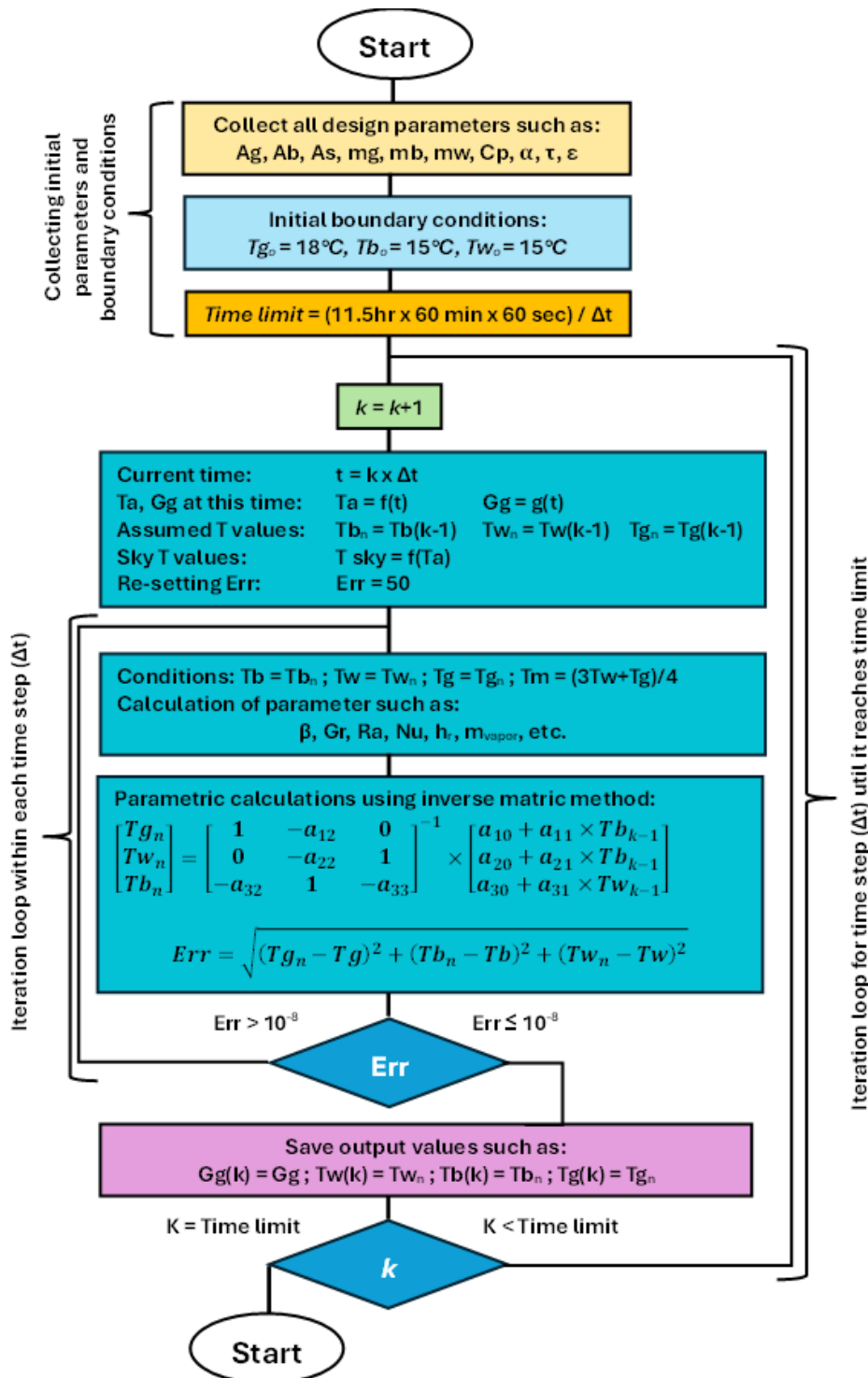
Fig. 7. Flow chart and algorithm of the solution procedure of the second model

3. Results and Discussion

This section presents the data values and variables gained by the two simulations. First, a comparison between the two models is thoroughly discussed. After that, the effect of each design parameter on the yield is explained, followed by a discussion on the effects and consequences of the assumptions made in these models.

3.1 First Model: Steady-State

The steady-state model is tested first using average values, where average solar radiation in Yemen is 500 cal/cm^2/day or 2.093e^{+07} J/m^2/day as reported by Ashwal [29]. Assuming 10 hours of sunshine for a sunny day, the average radiation intensity on a horizontal flat plate collector will be 581 J/m^2/s, which equates to 581 W/m^2. Using this averaged solar radiation intensity, the model is tested using ambient temperature of 25℃. For single basin single slope solar still design, following parameters are applied to this model as shown in Table 3. After that, the steady-state model is tested to calculate the distillate and accumulated yields using hourly-based values, utilizing ambient temperature and radiation intensity experimental data for a single day in Sana'a, Yemen from 6:00AM to 6:00PM. The calculated temperature profile at each part of the solar still for each hour during the day is illustrated in Figure 8 (a). Distillate mass yield in kg/h calculated for each hour during the day, followed by the calculated accumulated mass yield in kg which increased steadily throughout the day are shown in Figure 8 (b). The distillate water mass yield trend is well aligned with the increase in radiation intensity and temperature where maximum values are achieved at noon (12:30 PM) when sun zenith angle reaches zero before its starts to increase again resulting in a slightly accelerated drop in solar intensity and production yield.
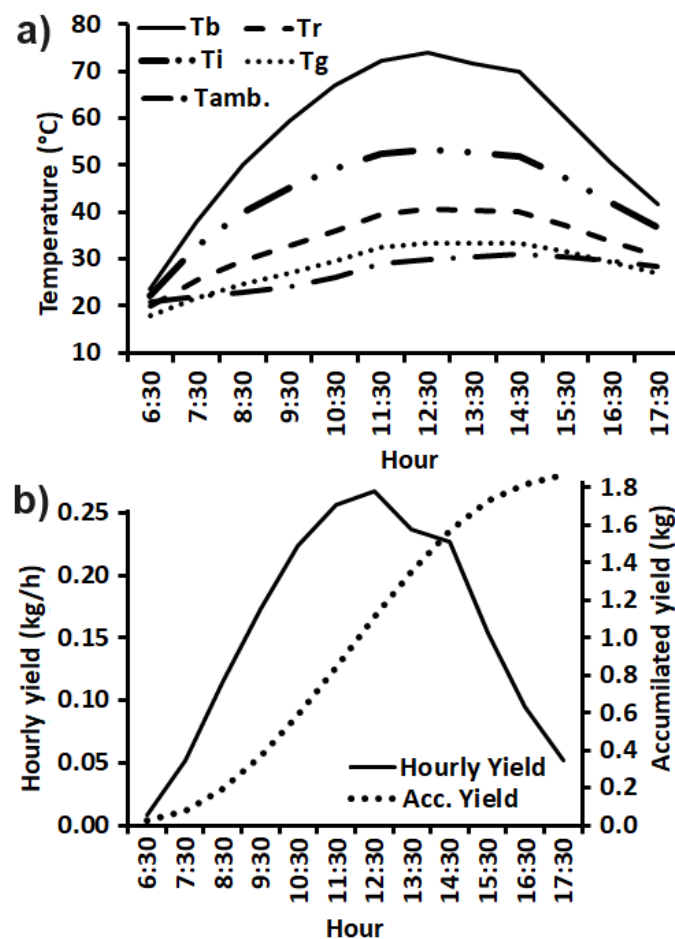
Fig. 8. Hourly profile of the solar still (a) Temperature (b) Mass yield

Table 3
Parameters of the first design and results obtained from the first model

Parameter	Value	Units	Description
Ab	0.32	m^2	Basin Area
Ag	0.3578	m^2	Glass area
Ak_air	0.576	m^2	Circumferential Area in contact with moist air
Ak_l	0.048	m^2	Circumferential Side Area in contact with water
Lc	37	$W/m.K$	Conductivity of the Basin liner material
Liz	0.04	$W/m.K$	Conductivity of the insulation (Polystyrene)
Lgal	0.08	$W/m.K$	Conductivity of the Ply-Wood
Dc	0.002	m	Thickness of the Basin plate
Diz	0.03	m	Thickness of the insulation
Dgal	0.02	m	Thickness of the wood plate
Results from first model			
Tb (basin)	60.7	°C	
Ti (interface)	46	°C	
Tg (glass cover)	27.8	°C	
Tr (moist air)	33.8	°C	
Distillate Yield	4.95e-05 =	kg/s	
	1.78	kg/day	

3.2 Second Model: Transient

Now these data were re-contrasted with the data obtainable from the second model which is the transient model. It must be noted that the initial temperatures (temperatures of the parts at the early morning) showed strong influence on the results. Initial temperatures of T_g =18°C, T_b =15°C and T_w =15°C were used for the calculations to match the experimental data. The input parameters of the transient model are summarised in Table 4.

Table 4
Input Parameters to the second model

Parameter	Value	Parameter	Value
$A_b = A_w (m^2)$	0.32	$U_{sw}(Wm^{-2}K^{-1})$	1.6
$A_{gc} (m^2)$	0.3578	$X_{ps}(m)$	0.03
$B_b (m)$	0.4	$X_{pw}(m)$	0.02
$h_{c,b-w}(W\,m^{-2}K^{-1})$	100	$\alpha_b(dimensoinless)$	0.96
$L_b(m)$	0.8	$m_g (kg)$	4
$m_b (kg)$	6	$m_w(kg)$	6.5
$U_{bo}(Wm^{-2}K^{-1})$	1.2		

The mathematical model is used to generate correlations that relates and can accurately predict the radiation intensity and consequently predict the ambient temperature pattern through reverse calculation as shown in Figure 9. The calculated correlation for radiation intensity throughout the day is shown in Eq. (58):

$$Gg = (1.68688e - 15) * time^4 - (1.5522019e - 10) * time^3 + (2.91320078643e - 6) * time^2 + 0.0299255740757829 * time - 6.537878369 \tag{58}$$

While the correlation for ambient temperature (Ta) is shown in Eq. (57):

$$Ta = -(5.12929e - 13) * time\textasciicircum3 + (2.17983e - 8) * time\textasciicircum2 - (1.65270e - 4) * time + 293.258$$
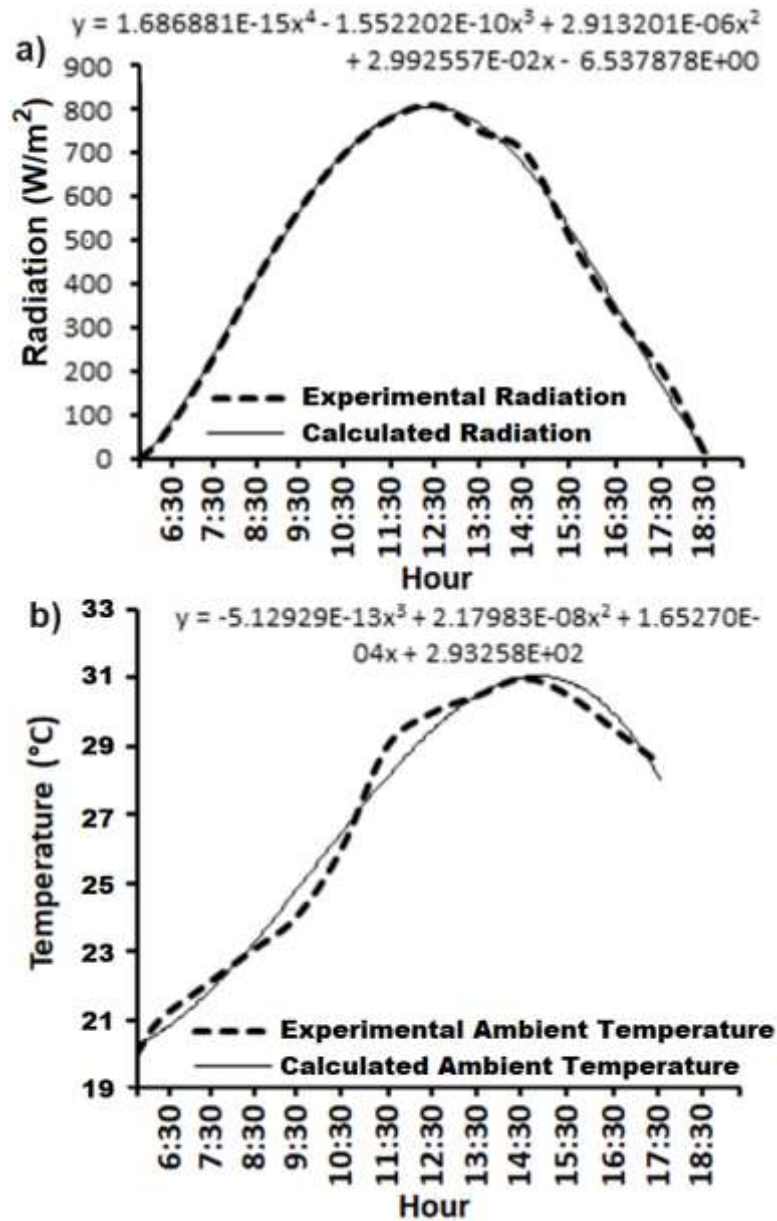
(59)

Fig. 9. Experimental data plot compared to the predicted correlation of (a) radiation (b) ambient temperature

Comparing the steady-state and transient models, the basin temperature (T_b), water temperature (T_w) and glass cover temperature (T_g) were compared as shown in Figure 10. The graph of variation of temperature with time of the second model is skewed to the right as shown in the temperature profile trends. In other words, temperatures attain their peak value at 2:00 PM, in contrast with the values attained from the first model which shows a peak temperature at 1:00 PM. In view of the fact that all components have energy fed to them nonstop, it is not strange for them to get further heated when the solar radiation starts to decrease at 1:00 PM. Actually, this behavior confirms experimental results provided by many researchers. The two models suggest different values of the water temperature. The reason behind this is that the first model calculates the interface temperature, while the second one evaluates the bulk temperature. Also, the time taken for the water

heating/cooling in the transient model is highly influenced by the amount of water in the basin or the basin depth due to the high heat capacity of water.
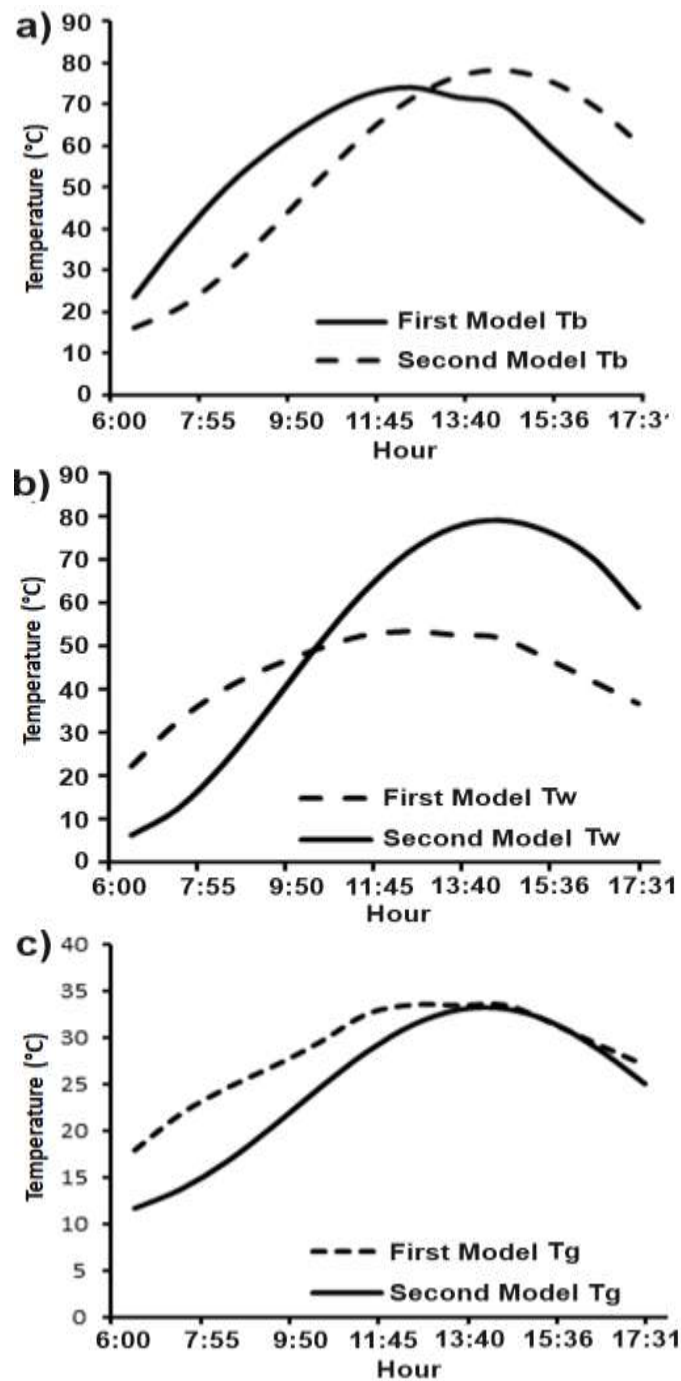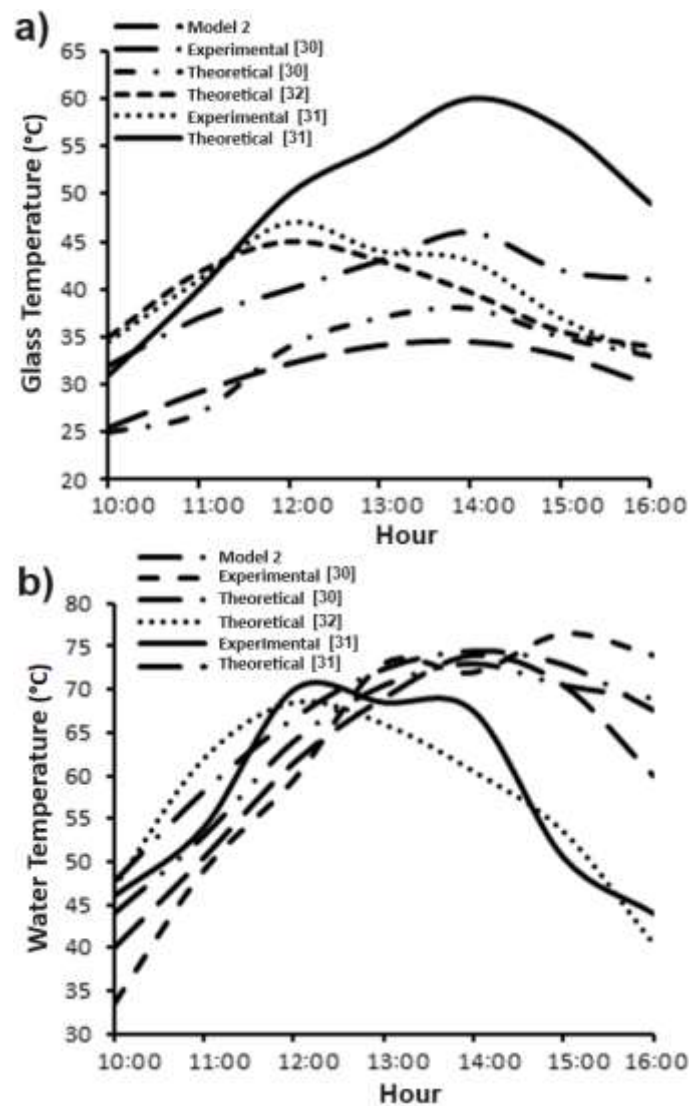

Fig. 10. (a) Basin temperature (b) Water temperature and (c) Glass cover temperature of both models

3.3 Verification of the Models

In this section, general verification of the temperature trends was discussed first followed by specific and in-depth verification of the second model (i.e., transient model). For the general verification, temperature trends of glass and water obtained from model 2 were compared to the temperature curves of other studies in literature [30-32] as shown in Figure 11. It should be noticed

that the geometry and operating conditions were not the same for all the compared studies. Water temperature T_b was in good agreement with the experimental results where peak temperature was in the range of 70-80°C during the period of 12:00-3:00PM, while other theoretical study [32] showed faster cooling rate due to the difference in water capacity in the basin. On the other hand, glass temperature T_g showed wider temperature range in general, due to the difference in glass area and ambient cooling effect. However, the current model was in good agreement with the two experimental studies with peak temperature in the range of 35-45°C, unlike the simulation findings in the other study [31] which reached up to 60°C.

Fig. 11. Second model compared to other theoretical and experimental studies in terms of (a) Glass temperature and (b) Water temperature

As for the in-depth specific verification of transient model in the current study, the model parameters were modified to match exactly the parameters in the reference study used as the verification source to achieve accurate comparison. Therefore, design parameters of the experimental setup proposed by the reference study by Ponar Ilker, [30] were implemented as the input variables into the transient model developed in the current study. These parameters are listed in Table 5 as obtained from the reference study.

Table 5
Parameters of the experimental design by the reference
[30] tested using second model

Parameter	Value	Unit
A_b	1	m^2
A_g	1.6	m^2
A_s	1	m^2
m_b	22.5	kg
m_w	15	kg
m_g	10	kg
$U_{bo}=U_{sw}$	0.1	W/m^2K
Cp_b	460	J/kgK
L	0.37	m

After that, values of incident solar radiation (G_g) and ambient temperature (T_a) are taken from graphs plotted by the reference study [30] and then the correlations relating G_g and T_a to time were calculated using the current model as shown in Eq. (60) and Eq. (61), respectively.

$$Gg = (1.540695e - 15) * time^4 - (1.368493e - 10) * time^3 + (2.21105e - 6) * time^2 + (3.838275e - 2) * time - (2.670479e + 1) \qquad (60)$$

$$Ta = -(3.847033e - 13) * time^3 + (1.733606e - 8) * time^2 + (2.350196e - 5) * time + 288.2203 \qquad (61)$$

Figure 12 shows a comparison of water and glass temperatures obtained by the second model with the experimental temperature values from the reference study. Water temperature predicted by the model was very close to the experimental values especially at the peak temperature period of 1:00-3:00PM with deviation < 10°C. The deviation in temperature was mainly caused by the temperature fluctuation in experiment mainly due to sudden changes in radiation intensity (due to clouds) and wind speed, while the fluctuation in these variables is not accounted for in the model. As for glass temperature, higher difference was notices in the range of 10-20°C, while the general trend remained similar reaching peak value at around 2:00PM. This larger difference could be attributed to several uncontrollable variables that can include the difference between condensation and evaporation rates, or more accurately the condensation potential compared with the evaporation potential. A fact that is not considered in the modelling procedure is that the evaporation rate is limited by the condensation potential at the other end, the glass; because of this the air would get heated along with the glass up to unpredictable values. Another important factor is the heat transmitted from the sides of the structure into the moist air, which heats it and in turn heats the glass as well. Moreover, unknown factors include the thickness and type of the glass which are not provided by the reference study and affects directly the heat conduction and storage inside the gas layers. Sudden changes in wind speed that cause external cooling is also uncontrollable and cannot be considered for the simulation.
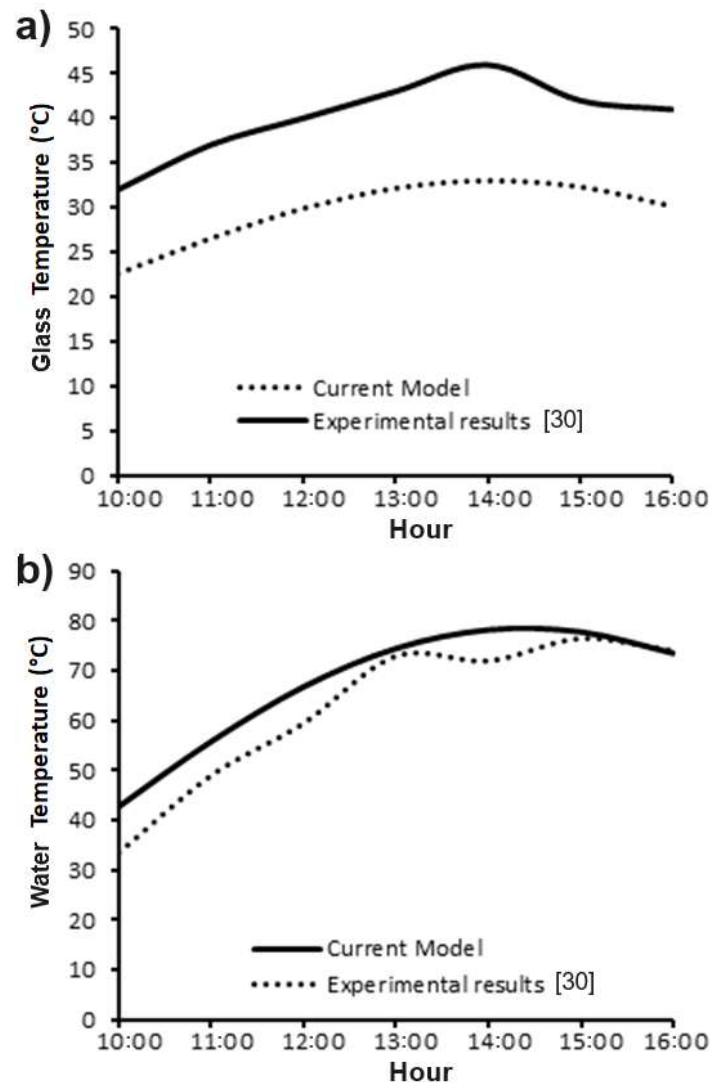
Fig. 12. Model verification using (a) glass and (b) water temperatures compared to the reference study [30]

4 Conclusions

The need to increase access to clean water cannot be overemphasized, so, the present investigation contributes toward resolving the shortage of clean water supply in Yemen. The current study presented a simple low-cost single slope solar still design for sea water desalination. Two mathematical models were investigated to predict the performance of the solar still. First model neglects the effect of time, assuming quasi-steady-state equilibrium, while the second model takes the time effect into account and applies the principle of lumped system analysis to simplify the solving procedure. The two models reported the same peak temperature for the basin and the glass cover. However, the time taken to reach this peak temperature is slightly different as predicted by each model. The transient model showed more realistic approximation of the temperatures and the peak time when validated and compared with other theoretical and experimental results from literature. It was concluded that the distillate water production yield is not only governed by the solar radiation intensity, but also strongly affected by basin and glass cover temperatures which are in tern highly influenced by the ambient temperature. It was also found that the ambient temperature is very influential on productivity. Thus, it is expected that productivity would increase in hotter climates and during summer. The hourly water production rate was shown to be almost linearly

proportional to the solar radiation intensity. Maximum production rate was about 0.27 kg/h at 12:30 PM in a typical hot summer day in Sana'a, Yemen, resulting in an accumulated water production of 1.9 kg/day. Future research will include the utilization of the mathematical model for the optimization of the solar still geometry and the experimental testing of the optimum geometry in Yemen.

References

[1] Ahmadi, Muhammad Aiman, Nurshafinaz Mohd Maruai, Mohd Fadzli Haniff, Ahmad Faiz Mohammad, Farah Mohd Redzuan, and Shahir Mohd Yusuf. "Numerical Investigation on Tandem Body Configurations in Prospect to Enhance Low Wind Energy Harvesting." *Semarak Engineering Journal* 3, no. 1 (2023): 9-13.

[2] Hao, Wong Kar, Mohd Afzanizam Mohd Rosli, Jayaprakash Ponnaiyan, Safarudin Ghazali Herawan, and Faridah Hussain. "A Simulation Study of Hybrid Solar Drying Chamber for Agriculture Product." *CFD Letters* 16, no. 9 (2024): 81-93. https://doi.org/10.37934/cfdl.16.9.8193

[3] M'hamed, Beriache, Hadj Henni Moustefa, Leila Mokhtar Saïdia, Bassam Gamal Nasser Muthanna, Ahmad Tajuddin Mohamad, and Nor Azwadi Che Sidik. "Experimental evaluation of the performance of a diesel engine feeding with ethanol/diesel and methanol/diesel." *Journal of Advanced Research in Experimental Fluid Mechanics and Heat Transfer* 15, no. 1 (2024): 14-27. https://doi.org/10.37934/arefmht.15.1.1427

[4] Al-Nehari, Hamoud A., Mahmoud A. Mohammed, Abdulkarem A. Odhah, K. A. Al-Attab, Bakeel K. Mohammed, Abdulwahab M. Al-Habari, and Nasr H. Al-Fahd. "Experimental and numerical analysis of tiltable box-type solar cooker with tracking mechanism." *Renewable Energy* 180 (2021): 954-965. https://doi.org/10.1016/j.renene.2021.08.125

[5] Noaman, Abdulla, Fadhl Ali Al-Nozaily, and Mohammed Hezam Al-Mashreki. Yemen Water Report, 2019.

[6] Berg, H. van den, S.J. van Meijeren, A. Gevaert, J. "Bazin Water availability in Yemen, Literature review of the current and future water resources and water demand in Yemen". United Nations Development Program, Final report. 2021.

[7] World Bank Report, "Highlights Challenges and Opportunities for Yemen's Economic Recovery and Growth", 2023.

[8] Huang, Lee Kai, Mirza Farrukh Baig, and Ervina Efzan Mhd Noor. "Innovative Solutions for Melaka's River Water Treatment." *Journal of Advanced Research in Fluid Mechanics and Thermal Sciences* 117, no. 2 (2024): 28-36. https://doi.org/10.37934/arfmts.117.2.2836

[9] Mir, Namra, and Yusuf Bicer. "Integration of electrodialysis with renewable energy sources for sustainable freshwater production: A review." *Journal of Environmental Management* 289 (2021): 112496. https://doi.org/10.1016/j.jenvman.2021.112496

[10] Moossa, Buzaina, Priyank Trivedi, Haleema Saleem, and Syed Javaid Zaidi. "Desalination in the GCC countries-a review." *Journal of Cleaner Production* 357 (2022): 131717. https://doi.org/10.1016/j.jclepro.2022.131717

[11] Shah, Kinnari M., Ian H. Billinge, Xi Chen, Hanqing Fan, Yuxuan Huang, Robert K. Winton, and Ngai Yin Yip. "Drivers, challenges, and emerging technologies for desalination of high-salinity brines: A critical review." *Desalination* 538 (2022): 115827. https://doi.org/10.1016/j.desal.2022.115827

[12] Le Quesne, W. J. F., L. Fernand, T. S. Ali, O. Andres, M. Antonpoulou, J. A. Burt, W. W. Dougherty et al. "Is the development of desalination compatible with sustainable development of the Arabian Gulf?." *Marine pollution bulletin* 173 (2021): 112940. https://doi.org/10.1016/j.marpolbul.2021.112940

[13] Prajapati, Mitul, Manan Shah, and Bhavna Soni. "A comprehensive review of the geothermal integrated multi-effect distillation (MED) desalination and its advancements." *Groundwater for Sustainable Development* 19 (2022): 100808. https://doi.org/10.1016/j.gsd.2022.100808

[14] Akaje, Wasiu, and B. I. Olajuwon. "Impacts of Nonlinear thermal radiation on a stagnation point of an aligned MHD Casson nanofluid flow with Thompson and Troian slip boundary condition." *Journal of Advanced Research in Experimental Fluid Mechanics and Heat Transfer* 6, no. 1 (2021): 1-15.

[15] Kumar, Aditya. "ANSYS Fluent-CFD analysis of a continuous single-slope single-basin type solar still." *Green Technologies and Sustainability* (2024): 100105. https://doi.org/10.1016/j.grets.2024.100105

[16] Essa, Fadl A., Mahmoud M. Othman, A. S. Abdullah, M. M. Younes, Z. M. Omara, and Hesham Khalil. "Testing the performance of tubular solar still with flat basin, cords wick basin, and various angle of inclinations." *Results in Engineering* (2024): 102406. https://doi.org/10.1016/j.rineng.2024.102406

[17] Abdulridha, Hussein Oleiwi, Hassanain Ghani Hameed, and Basil Noori Merzah. "Performance Study for Single Slope Solar Still Integrated with Different Types of Solar Collectors." *Desalination and Water Treatment* (2024): 100538. https://doi.org/10.1016/j.dwt.2024.100538

[18] Sahota, Lovedeep, and G. N. Tiwari. "Exergoeconomic and enviroeconomic analyses of hybrid double slope solar still loaded with nanofluids." *Energy Conversion and Management* 148 (2017): 413-430. https://doi.org/10.1016/j.enconman.2017.05.068

[19] Sharshir, Swellam W., M. A. Rozza, Marwan Elsharkawy, M. M. Youns, Fawzy Abou-Taleb, and A. E. Kabeel. "Performance evaluation of a modified pyramid solar still employing wick, reflectors, glass cooling and TiO2 nanomaterial." *Desalination* 539 (2022): 115939. https://doi.org/10.1016/j.desal.2022.115939

[20] Saxena, Abhishek, Erdem Cuce, A. E. Kabeel, Mohamed Abdelgaied, and Varun Goel. "A thermodynamic review on solar stills." *Solar Energy* 237 (2022): 377-413. https://doi.org/10.1016/j.solener.2022.04.001

[21] Rabhi, Kamel, Rached Nciri, Faouzi Nasri, Chaouki Ali, and Habib Ben Bacha. "Experimental performance analysis of a modified single-basin single-slope solar still with pin fins absorber and condenser." *Desalination* 416 (2017): 86-93. https://doi.org/10.1016/j.desal.2017.04.023

[22] Abbaspour, Mohammadreza, Abas Ramiar, and Qadir Esmaili. "Efficiency improvement of vertical solar stills–A review." *Solar Energy* 235 (2022): 19-35. https://doi.org/10.1016/j.solener.2022.02.027

[23] Omara, Z. M., Wissam H. Alawee, Ali Basem, and Alaa Dhari Jawad Al-Bayati. "Heat loss reduction techniques for walls in solar stills: A review." *Results in Engineering* (2024): 101996. https://doi.org/10.1016/j.rineng.2024.101996

[24] Madhlopa, A., and C. Johnstone. "Numerical study of a passive solar still with separate condenser." *Renewable Energy* 34, no. 7 (2009): 1668-1677. https://doi.org/10.1016/j.renene.2008.12.032

[25] Duffie, John A., and William A. Beckman. *Solar engineering of thermal processes*. New York: Wiley, 1980.

[26] Ya, Cengel, A. Ghajar, and H. Ma. "Heat and mass transfer fundamentals & applications." *McGraw-Hill* (2015).

[27] Incropera, Frank P. "Principles of Heat and Mass Transfer." (2013).

[28] Zurigat, Yousef H., and Mousa K. Abu-Arabi. "Modelling and performance analysis of a regenerative solar desalination unit." *Applied thermal engineering* 24, no. 7 (2004): 1061-1072. https://doi.org/10.1016/j.applthermaleng.2003.11.010

[29] Al-Ashwal, M. Ali. "All renewable energy applications in Yemen are best practice." *ISESCO Science and Technology Vision* 1, no. 1 (2005): 45-50.

[30] Alkan, Pınar İlker. *Theoretical and experimental investigations on solar distillation İYTE Gülbahçe Campus area seawater*. Izmir Institute of Technology (Turkey), 2003.

[31] Madhlopa, Amos. "Development of an advanced passive solar still with separate condenser." PhD diss., The University of Strathclyde, 2009. https://doi.org/10.1016/j.renene.2008.12.032

[32] Panchal, Hitesh, and Pravin Shah. "Modelling and verification of single slope solar still using ANSYS-CFX." *International Journal of Energy and Environment* 2, no. 6 (2011): 985-998.